npj | natural hazards

Article

https://doi.org/10.1038/s44304-025-00100-8

Assessing infrastructure exposure to mountain wave wind events in the Southern Appalachians

Check for updates

Marcus D. Williams[1] ✉, Bradford D. Johnson[2], Zachary Cope[1], Craig Ramseyer[3], David Hotz[4] & Jeremy Buckles[4]

Mountain wave wind events (MWWE) pose significant risks to infrastructure, particularly in mountainous regions with extreme downslope winds exceeding 40 m s^{-1}. Although extensively studied in the western U.S., MWWE impacts remain underexplored in the Southern Appalachians, where critical energy infrastructure intersects high-risk areas. This study utilizes high-resolution Weather Research and Forecasting (WRF) model simulations to analyze probable MWWE recurrence and assess transmission line vulnerability. Seven MWWE spanning 41 h at 500-m resolution were modeled, identifying strong correlations between elevation and High Wind Warning-level wind exceedances ($|U| \geq 17.8$ m s^{-1}), predominantly near ridgelines and downwind slopes. Transmission lines at higher elevations and select valleys experience repeated threshold-level wind exposure, highlighting risks of infrastructure failure and cascading hazards like wildfires. Results underscore the necessity for enhanced risk mitigation, grid resilience, and adaptive infrastructure planning. This research advances MWWE's understanding in the Eastern U.S. and provides actionable insights for stakeholders.

Fluctuations in climate variability are projected to increase the intensity and frequency of extreme weather events, including extreme wind events like mountain wave wind events (MWWE)[1,2]. These events, generated by stable airflow over topographic barriers, pose significant threats to infrastructure and wildland fire management, as they can generate surface wind speeds greater than 50 m/s[3].

When air is advected over mountain ranges, stationary wave disturbances, commonly referred to as mountain waves, are produced in atmosphere[3]. Mountains are capable a producing a range of downslope wind regimes depending on coincident atmospheric static stability, background flow regime, and the width and height of the barrier[4,5]. In situations with strong cross-mountain flow, coupled with enhanced static stability at low-levels, mountain waves are often present and can lead to strong downslope wind gusts (i.e., MWWE) in excess of 40 m/s observed across many mountain chains, including both the Rocky and Appalachian Mountains[6–10]. MWWE of slightly lower magnitude have also been noted in areas of the U.S. with significantly lower elevation, including mountain wave-induced gusts of 30 m/s immediately downwind of High Point, New Jersey (elevation 550 m) in the Kittatinny Mountains[11]. The non-convective winds produced by mountain waves can lead to large tree falls, power outages, and property damage[7,9,10]. Terrain-induced wind gusts have also been associated with fatalities, representing ~6% of all non-convective wind fatalities in the U.S.[12]. In addition to surface-based hazards, mountain waves are commonly associated with severe clear-air turbulence, which can lead to fatal aviation incidents[8,13]. Lee-side mountain waves have also been linked to the formation of rotors, contributing to numerous aircraft accidents[14].

Many theoretical and computational studies over the last four decades have advanced the understanding of mountain wave generation and its translation to surface wind gusts. Linear and nonlinear theories have been employed to elucidate these processes. For example, sharp low-level temperature inversions can reflect vertically propagating gravity waves. Klemp and Lilly[15] demonstrated that the depth, height, and temperature difference across an inversion play critical roles in determining downslope wind speed. In addition to temperature inversions, internal gravity waves have been suggested to reflect off levels of the troposphere where the cross-barrier flow component goes to zero (so-called critical levels)[16]. Wave breaking has also been found to play an important role in some downslope wind events[17,18]. In the absence of a critical level, mountain waves can trap gravity wave energy within the underlying flow, effectively imposing an upper boundary condition similar to a critical level[19]. Research has shown that downslope

[1]Athens Prescribed Fire Lab, USDA Forest Service, Southern Research Station, Athens, GA, USA. [2]Department of Geography, Florida State University, Tallahassee, FL, USA. [3]Department of Geography, Virginia Polytechnic Institute and State University, Blacksburg, VA, USA. [4]National Weather Service (NWS) Morristown WFO, Morristown, TN, USA. ✉e-mail: marcus.d.williams@usda.gov

windstorms increase in magnitude and likelihood when a critical layer and/or wave breaking is present[6,9,11,18]. Nonlinear interactions are responsible, at least in part, for the generation of downslope windstorms in response to mountain wave generation[6,18,20]. An example of this nonlinearity is the existence of a critical Froude (Fr) threshold where the flow surmounting topography transitions from subcritical (Fr < 1) to supercritical (Fr > 1) flow, representing a conversion of potential to kinetic energy and increasing wind speeds downslope[6,18]. One of the most thorough investigations of nonlinearities highlighted the role of the strength and vertical position of the temperature inversion in the magnitude of the downslope MWWE[20]. With weak inversions, numerical experiments show no low-tropospheric reflection of the vertically propagating gravity (mountain) waves[20]. However, strong inversions, particularly when they are situated directly above the mountain top, were capable of producing a continuum of responses including trapped lee waves, lee waves with rotors, and hydraulic jumps[11,20,21]. These hydraulic jumps represent the most severe and extreme MWWE.

While MWWE have been extensively studied in the western United States, their potential impacts in the Appalachian region[9,21–26] warrant continued investigation, particularly concerning critical infrastructure like energy transmission lines. This knowledge gap poses challenges for climate adaptation and disaster risk reduction efforts in the region. Recent events have underscored the vulnerability of infrastructure to MWWE in the Appalachians. The destructive 2016 Chimney Tops 2 fire in the Great Smoky Mountains National Park was exacerbated by extreme winds and downed power lines, resulting in widespread damage and loss of life[27]. Similarly, the 2021 Marshall Fire in Boulder, Colorado, highlighted the devastating consequences of wildfires ignited by wind-damaged transmission lines[28,29]. These events emphasize the urgent need to assess and mitigate the risks posed by extreme winds, including but not limited to MWWE, to critical infrastructure in vulnerable regions.

The Weather Research and Forecasting (WRF) modeling system[30] and its predecessor, The Pennsylvania State University–NCAR Mesoscale Model version 5 (MM5), have been extensively used to investigate MWWE and their impacts[31–33]. These studies highlight WRF's capability to capture mountain wave dynamics, including the influence of model parameters and topography on wave characteristics. Oltmanns et al.[34] further emphasized the importance of model resolution in accurately simulating mountain wave events and their impacts on wind speed.

This study aims to enhance understanding of MWWE by assessing their potential impact on transmission line infrastructure in the Southern Appalachians. Specifically, we aim to:

- *Characterize* the occurrence of MWWE in the Southern Appalachians during identifiable high-wind scenarios using high-resolution WRF simulations.
- *Identify* areas of high MWWE exposure coincident with transmission line infrastructure.
- *Assess* the vulnerability of transmission line infrastructure to MWWE-induced wind damage.

By providing a detailed evaluation of MWWE risks to transmission line infrastructure, this research contributes to improved risk assessment, infrastructure planning, and wildfire mitigation strategies in the Southern Appalachians. By characterizing MWWE recurrence, identifying high-exposure areas, and assessing transmission line vulnerability, this study offers a comprehensive analysis beyond previous case studies or idealized simulations. Using high-resolution WRF simulations, we assess a range of probable MWWE events, delivering insights for policymakers, utility companies, and emergency managers working to strengthen critical infrastructure resilience amid grid modernization and a variable climate.

Results

Model-scale analysis

An initial characterization of the recurrence of MWWE in the Southern Appalachians was performed using the Advanced Research WRF model, which provided numerical simulations of seven suspected MWWE in the domain. These seven simulations span 506 cumulative hourly timesteps at 500-m horizontal resolution. WRF was configured using the NCAR convection-permitting physics suite and 40 vertical levels and a pressure level top of 50 pascals in the model (complete model configurations are provided in Table 1).

An initial characterization of the recurrence of MWWE in the Southern Appalachians was performed. The Weather Research and Forecasting (WRF) Advanced Research WRF model was used to provide numerical simulations of seven probable MWWE in the domain. These seven simulations span 506 cumulative hourly timesteps at 500-m horizontal resolution. WRF was configured using the NCAR Convection-Permitting Suite (https://www2.mmm.ucar.edu/wrf/users/physics/wrf_physics_suites.php) and 40 vertical levels in the model. The complete WRF model configurations are provided in Table 1.

A total of 6.33×10^7 modeled grid points were evaluated across the seven simulations. Wind speeds at 10-m height above ground level were simulated. For each event (Table S1), the dates corresponding to the top three simulated 10-m winds were determined. The hourly timesteps ($N = 41$) for each date surrounding these higher-end events, or extracted timesteps (ET), are assessed more closely. All subsequent analysis focuses on the ET simulations. Figure 1 provides the maximum gridded 10-m wind across the ET at each grid point; the maximum 10-m wind speeds range from 5.4 to 35.4 m s^{-1}. The simulated 10-m wind speeds are computed at each grid point for every discrete time step according to the finite difference formulation of the WRF model. These values should be interpreted as point-wise instantaneous estimates rather than spatial or temporal averages over the grid cell or time step and likely do not fully capture peak wind gusts that may occur on smaller spatial and temporal scales. It is reasonable to presume that true peak winds, particularly above the surface, exceed the modeled 10-m winds. Figure 2 shows the distribution of 10-m wind maxima exceeding 17.8 m s^{-1} (~40 mph) across the domain. These "exceedances" are not categorized explicitly as MWWE but possess impact similarities with MWWE as presently understood in the literature and correspond to regional high-wind warning criteria as defined by the National Weather Service[35]. Critically, wind speed magnitudes above this threshold have been associated with an increased risk of transmission line failure[36,37]. A total of 92,326 grid cells (<0.1% of all modeled points) exceeded the 17.8 m s^{-1} threshold. Of the simulated 41 h, the maximum number of hours of exceedance at any given grid point was 15 (see Fig. 2).

Concentrated areas with hours of exceedance between three and five are shown near the Tennessee-North Carolina border, with smaller pockets of recurrence found near ridgelines throughout the domain. To emphasize spatial variability and density of exceedances with respect to terrain (Fig. S1), Table 2 shows the distribution of threshold-level grid points by elevation. While the majority of threshold exceedances are below 700 m, these are distributed over a much larger area (>384,000 km^2) that equates to 85 percent of the total model domain area. Above 700 m, recurrences are more frequent spatially. For example, the elevation band between 1000 and 1300 m had 15,689 exceedances while only encompassing approximately 2% of the modeled domain. This results in a much higher ratio of 1.4 exceedances per km^2 at this higher elevation band when compared to a ratio of 0.1 for the area below 700 m. A comparison of the data using the Pearson correlation coefficient suggests a strong covariance between elevation and number of exceedances per km^2; a correlation coefficient of 0.89 is returned on a scale of −1 to 1, with values closer to one being indicative of a strong positive relationship.

The threshold maxima are frequently located downwind of the higher ridges, which is suggestive of MWWE. The location of these maxima with respect to elevated positions (or mountain ridges) varies with wind direction, which governs the orientation of the windward and leeward positioning. Wind roses aggregated by threshold wind speeds across the eight states within the Southern Appalachians provide a characterization of the prevailing surface wind directions (Fig. 3). Wind rose directional bins are provided in 16 bins of 22.5° width and indicate a high number of exceedances in Tennessee ($N = 30{,}628$) and the high frequency of southwesterly wind direction domain-wide. Each state has custom scales due to a wide disparity in modeled threshold exceedances. The least number of exceedances is found in South Carolina ($N = 2$) over the chosen study hours. The North Carolina and Virginia figures indicate a secondary maxima in modeled wind event directions from the southeasterly quadrant. While this secondary maxima is not immediately evident in Tennessee, raw counts in southeasterly bins (123.75°–168.75°) total 958 grid cell exceedances. This reorientation of the windward-leeward positioning in a southeasterly regime places the excessive winds on the western side of the highest ridges and is counter to the predominant west-southwesterly direction.

Table 1 | Configuration of WRF Version 4.3 Model Physics and Parameterization Scheme

Model physics	Parameterization scheme
Microphysics	Thompson
Cumulus	Tiedtke
Longwave radiation	RRTMG
Shortwave radiation	RRTMG
Boundary layer	MYJ
Surface Layer	MYJ
Land Surface	Unified Noah LSM

County-scale analysis

Localized preparedness and response to extreme wind hazards are often carried out by a range of practitioners, including emergency managers and local NWS Weather Forecast Offices, who operate within prescribed political jurisdictions. County-level data is commonly used to facilitate these activities. The recurrence of the exceedance events is derived from Fig. 2 and aggregated for use at the county-level (Fig. 4). A relative maxima surrounds the southern border of Tennessee and North Carolina. In general, the county-scale depiction tracks the exceedance-elevation relationship discussed earlier; valleys have minimal occurrences while exceedances increase near ridges. One exception is the higher ridges of western North Carolina in the set of counties removed from the border. While exceedances are observed, the modeled events do not produce maximum winds at the same rate as similar elevations near the aforementioned border.

Infrastructure exposure

The tangible impacts of the exceedances may be manifest in energy infrastructure exposure. By combining the number of exceedance hours at each grid point with active transmission lines, a depiction of vulnerable utilities is shown in Fig. 5. This figure focuses on the area of highest recurrence near the

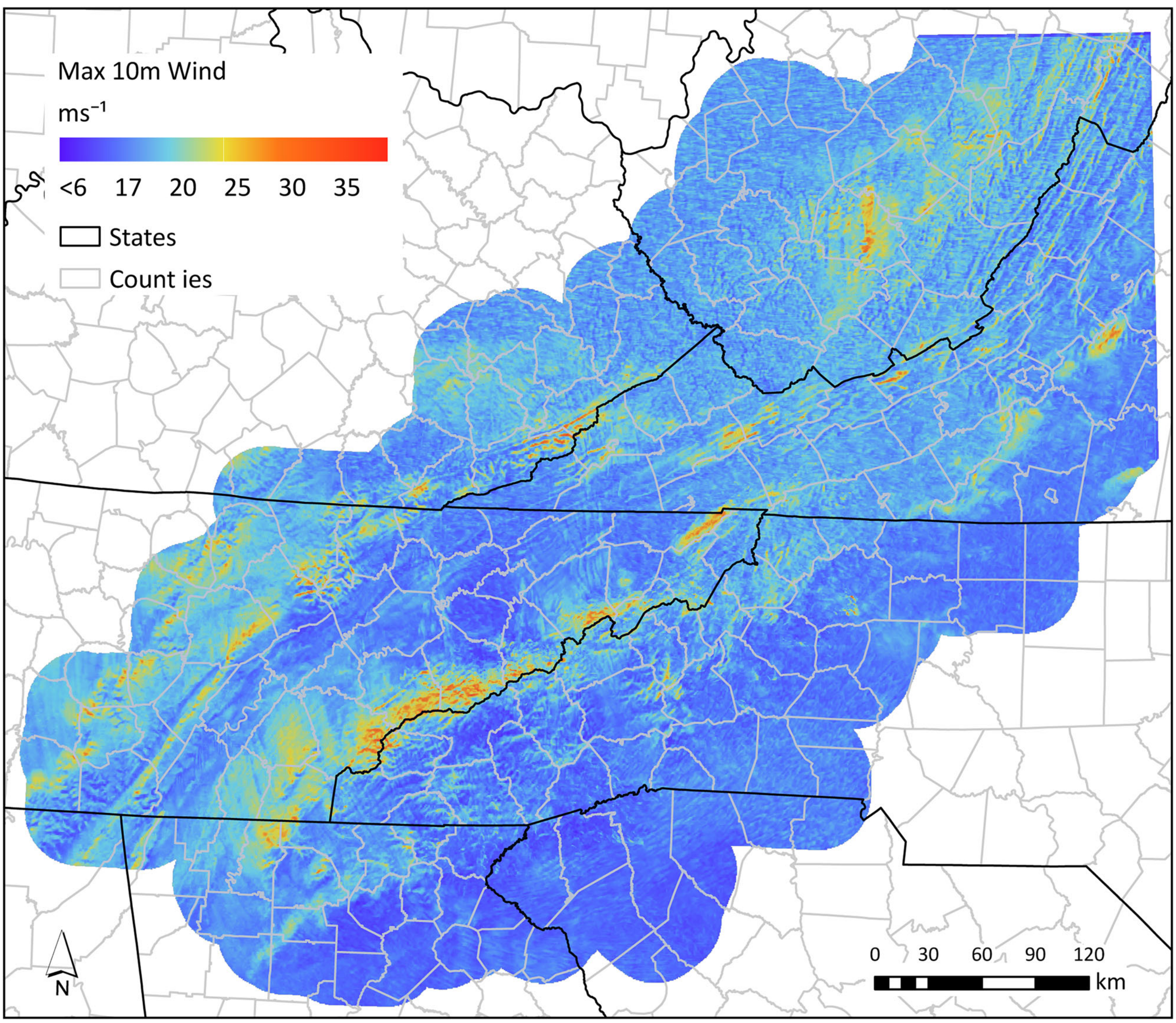

Fig. 1 | Maximum simulated 10-m wind speed (|**U**|) at each grid point over extracted modeled timesteps.

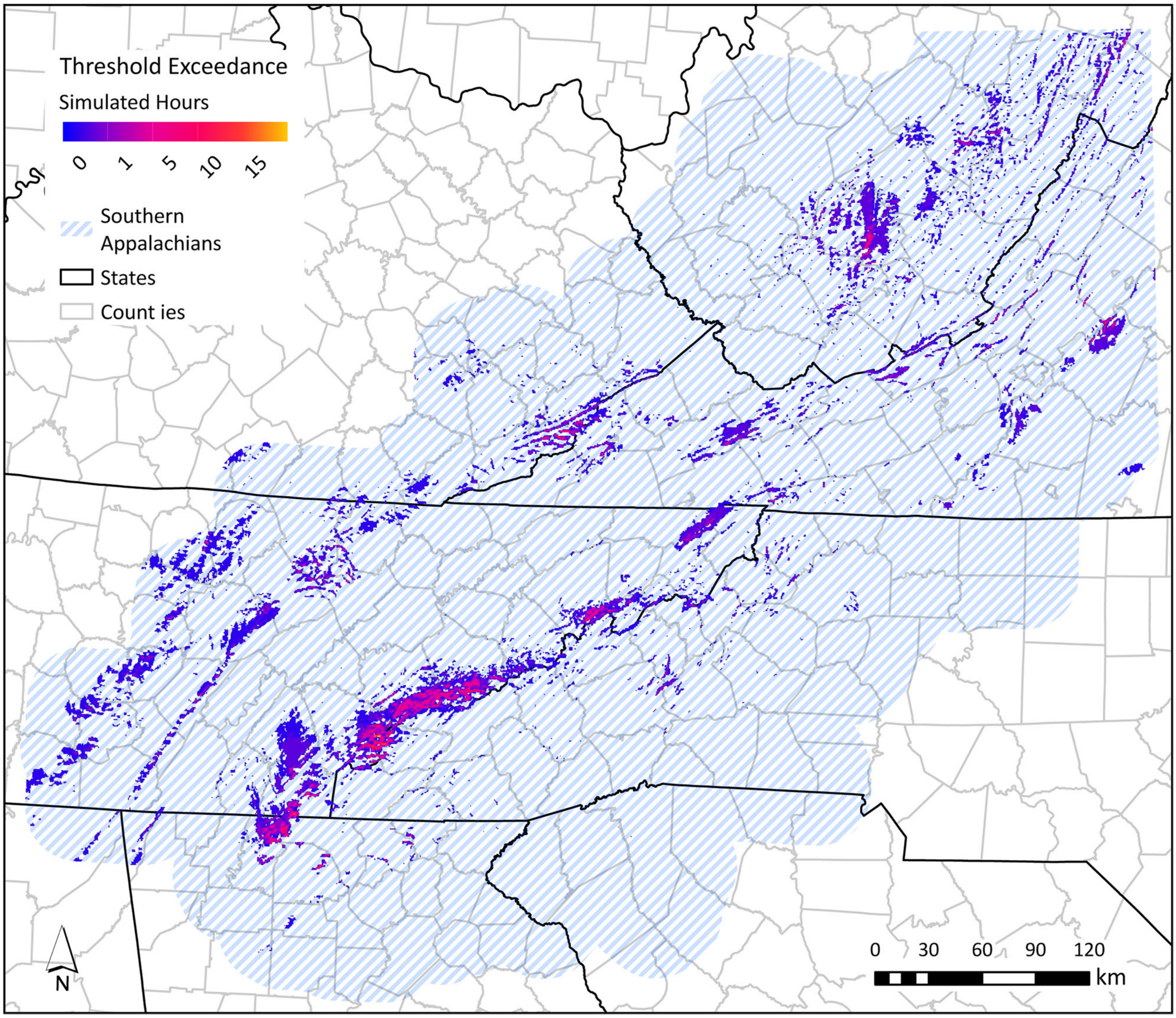

Fig. 2 | Number of threshold ($|\mathbf{U}| \geq 17.8$ m s^{-1}) exceedances across all extracted timestep simulations by grid point in the domain.

Table 2 | Summary of the WRF model domain and wind speed exceedances across five elevation bands

Elevation band (m)	Exceedance count	Total contoured area (km^2)	Ratio to total domain area	Exceedances per km^2
<700	43,965	384,297	0.849	0.10
701–1000	27,123	37,482	8.28×10^{-2}	0.72
1001–1300	15,689	11,138	2.46×10^{-2}	1.41
1301–1600	4600	1758	3.89×10^{-3}	2.61
1601–1900	949	232	5.13×10^{-4}	7.68

The exceedance count represents the total number of grid cells where simulated wind speeds in extracted timesteps exceed 17.8 m s^{-1}. Exceedances per km^2 quantify the density of exceedances within each elevation band, calculated as the exceedance count divided by the total contoured area.

Tennessee–North Carolina border. As expected, the transmission lines subject to repeated (or prolonged) incidents of exposure are in higher elevations. However, a number of exposed transmission lines are also present in valleys. As stated earlier, the peak simulated winds over the exposed lines are likely underestimates of actual peak winds during the modeled events. Given this perspective, it is plausible that more transmission lines are subject to threshold-level wind gusts than are shown here.

Discussion

This study provides a novel assessment of MWWE and their potential impacts on transmission line infrastructure in the Southern Appalachians, contributing to a critical but underexplored area of research. Through high-resolution WRF model simulations, we characterized MWWE recurrence, identified regions of high exposure, and assessed the vulnerability of critical infrastructure. Our findings highlight both the localized and systemic risks associated with these events and underscore the need for proactive risk mitigation strategies considering climate variability.

The simulations suggest that MWWE recurrence and severity are strongly influenced by topographic features, with the highest wind speed exceedances concentrated near ridgelines and downwind of elevated terrain. This aligns with previous studies in other mountainous regions, which emphasize the role of terrain-induced wave dynamics in generating extreme surface winds[31,38]. The Southern Appalachians, however, present unique challenges due to the dense vegetation, interconnected valleys, and proximity of critical infrastructure to vulnerable areas.

The relationship between elevation and MWWE-induced wind speeds was evident, with exceedances per square kilometer increasing significantly above 700 m. This elevation threshold is particularly relevant for infrastructure planning, as transmission lines and other critical facilities often traverse elevated terrain. Our results indicate that regions near the Tennessee–North Carolina border are hotspots for MWWE exposure,

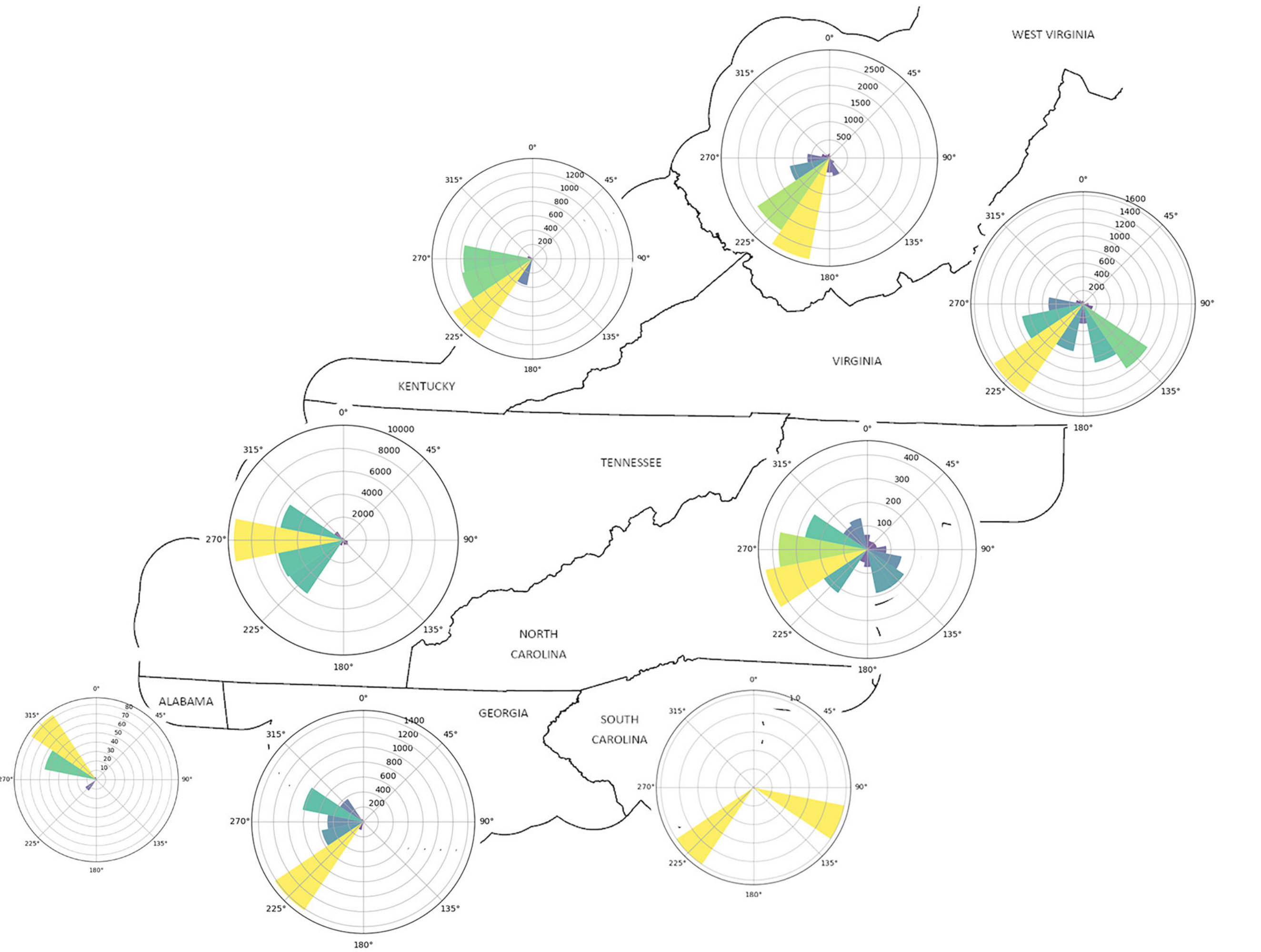

Fig. 3 | Aggregated, binned wind direction by state across the domain during simulated grid point threshold exceedances ($|U| \geq 17.8\ \mathrm{m\ s^{-1}}$). Inner scales of exceedance count change depending on the maximum *N* exceedances in each geographical division.

suggesting that these areas may require targeted adaptation measures to mitigate risks.

The vulnerability analysis demonstrated that transmission lines are disproportionately exposed to MWWE in higher elevations, with several lines experiencing repeated or prolonged periods of high wind speeds. While our analysis focused on 10-m simulated winds, actual transmission line heights, often exceeding 30 m, are likely subjected to even greater wind stresses. This finding suggests that current models may underestimate the true risk to infrastructure. Additionally, valleys also exhibited some exposure, which may be attributed to complex flow interactions and localized wind amplification.

The implications of MWWE extend beyond direct infrastructure damage. The potential for wind-induced failures to spark wildfires, as evidenced by events like the Chimney Tops 2 fire, underscores the need for integrated risk assessment frameworks that consider both direct and cascading hazards. Given the increasing frequency of extreme weather events associated with climate variability, the resilience of the Southern Appalachian energy grid is an urgent priority.

While this study provides valuable insights, several limitations warrant consideration. First, the simulations were based on a select set of probable MWWE events rather than a climatological analysis. Expanding the dataset to include a broader range of MWWE across multiple seasons and years would provide a more comprehensive understanding of their recurrence and impacts. Second, while the WRF model was configured with high spatial resolution, additional sensitivity studies could help refine the influence of specific model parameters on MWWE dynamics.

The remote nature of the Southern Appalachians and a sparse environmental observation network limit model verification options. Future research should also explore the integration of observational data, such as from remote sensing or in situ wind measurements, to validate and improve model outputs. Additionally, the development of predictive tools for real-time MWWE monitoring could enhance early warning systems, enabling more effective mitigation measures. Finally, studies focusing on the economic and social dimensions of MWWE, such as the cost of infrastructure retrofits or the impact on energy reliability, would complement the physical analyses presented here.

While the current study focuses on the horizontal spatial exposure of critical infrastructure to MWWE—using high-resolution 10-m wind speed outputs from a finite difference WRF configuration—we recognize the importance of further investigating the vertical structure of these events. Our analysis did not include detailed vertical sensitivity studies, which would be necessary to confirm that the simulated vertical wind profiles truly conform to the established dynamics of downslope windstorms. In future work, we plan to conduct dedicated vertical sensitivity analyses that evaluate the effects of vertical resolution, parameterization differences, and model top configuration within the WRF framework. This in-depth examination of vertical wind profiles will enhance our understanding of MWWE dynamics. Ultimately, these efforts aim to improve our ability to predict and mitigate the impacts of downslope windstorms on critical infrastructure.

Despite these limitations, this study contributes to the growing body of knowledge on MWWE and their potential impacts on infrastructure. The findings underscore the need for proactive measures to enhance the

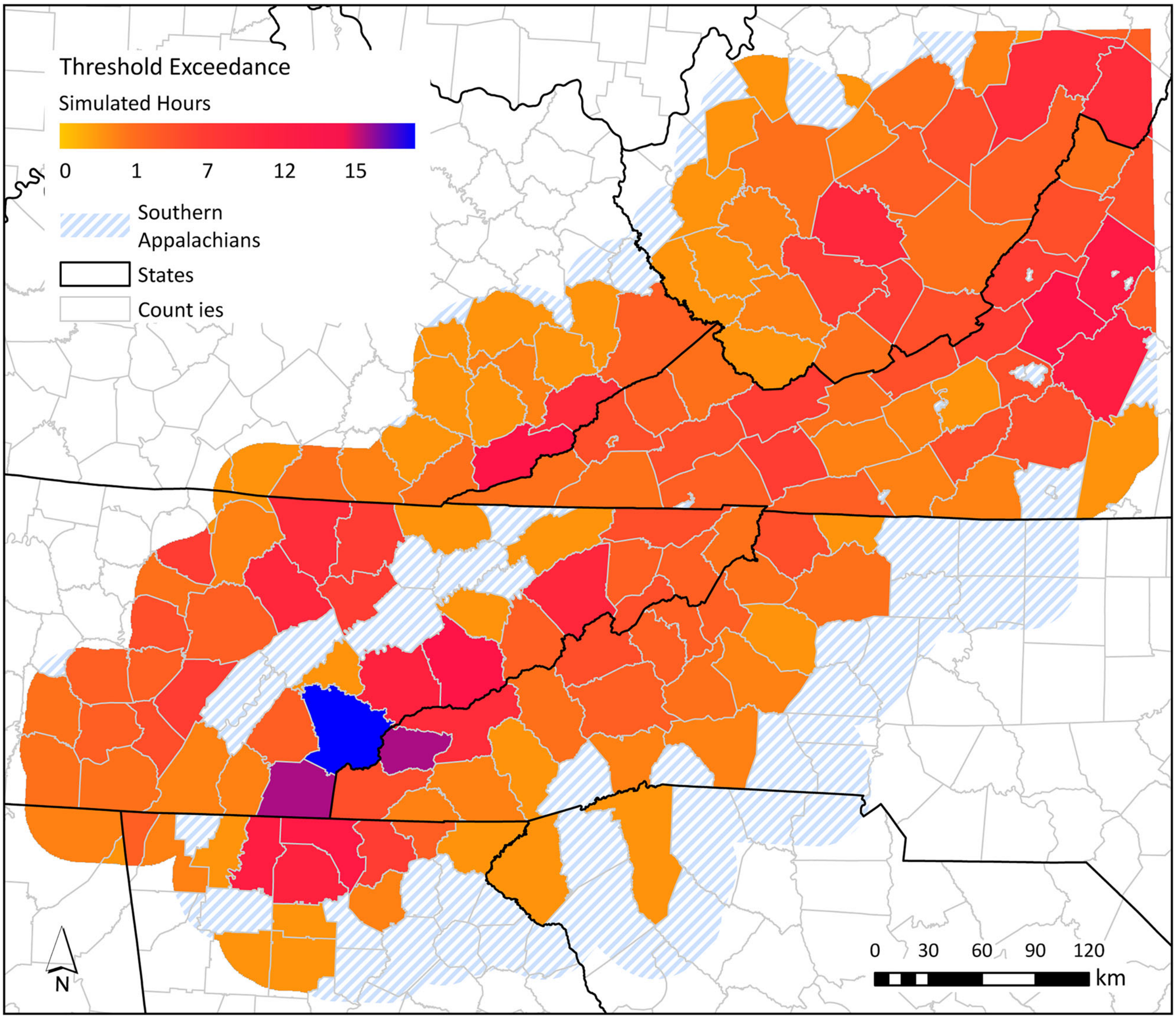

Fig. 4 | County-aggregated hourly exceedances across all extracted simulated timesteps.

resilience of critical infrastructure in the face of increasing MWWE risk. This research can inform the development of effective adaptation strategies to protect infrastructure and communities from the adverse effects of MWWE in the Southern Appalachians.

Methods

Study area

The Southern Appalachians are herein defined by the mountainous region in the eastern United States south and west of a vertex roughly centered at 39.0°N, 79.2°W extending from West Virginia to a terminal vertex (33.1°N, 87.5°W) in northern Alabama. The domain is finalized by applying a 30-km buffer around a 700-m elevation contour (Fig. 6). It encompasses a contiguous area of approximately $2.08 \times 105\ \mathrm{km}^2$ with mean and maximum elevations of 538 m and 1909 m, respectively. The northeast-to-southwest-oriented mountain chain is characterized by a system of anticline-syncline pairs with elongated ridges and valleys within a broader plateau. The region resides in a humid subtropical climate with subtle variations in temperature gradients surrounding the higher ridges. The seasonal climate regimes are governed by the latitudinal migration of the subtropical high. Mid-latitude westerlies dominate storm tracks over at least part of the region year-round, with diminishing influence in southern sections during the summer season (June to August). The land cover is predominantly mixed deciduous and pine forest; smaller urban areas are situated within valleys, while larger metropolitan areas flank the southern plateau, creating increased exposure to the wildland–urban interface.

Data

A series of probable MWWE were identified by operational meteorologists at NWS Morristown (personal communication). These events span the years 2011 to 2018. Given the lack of a viable observation network over the domain, a modeling investigation was deployed. The Advanced Research WRF (WRF–ARW) is a fully compressible, nonhydrostatic numerical modeling suite and has been deployed extensively to investigate the physics and dynamics of atmospheric phenomena. The model is particularly useful in applications of high-impact weather coincident with a lack of real-time observational capabilities. In this study, WRF–ARW simulates the atmospheric environment and provides hourly outputs of modeled variables over the domain. The boundary conditions were initialized using the National Centers for Environmental Prediction gridded, 12-km North American Mesoscale model. An initial inner domain was downscaled to 4 km while the innermost domain was simulated at 500 m horizontal spatial resolution.

US Census/TIGER shapefiles provide political boundaries from the state to the county level. Transmission line infrastructure data was obtained from the Geospatial Management Office of the U.S. Department of Homeland Security. A combination of WRF–ARW model output, Python

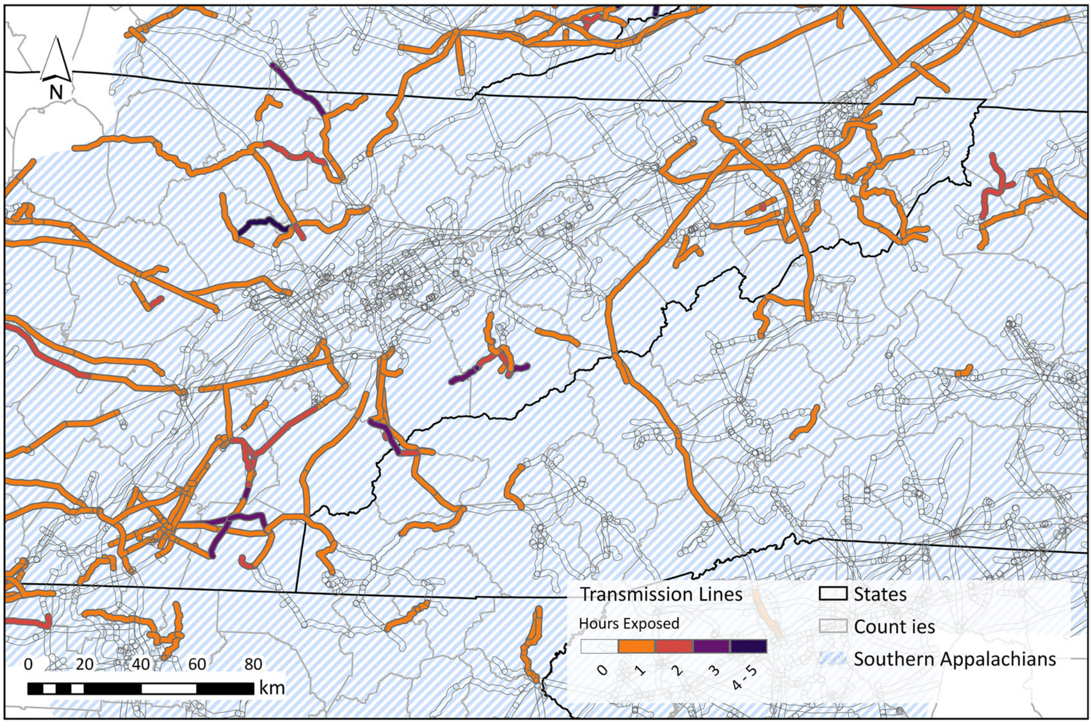

Fig. 5 | Energy transmission lines and the total hours of exposure to threshold-level simulated winds. Hours of exposure were determined by aggregating 10-m wind speeds exceedances ($|\mathbf{U}| \geq 17.8$ m s^{-1}) that intersect with 1-km transmission line buffers. Note that actual transmission line heights often exceed 10 m above ground level.

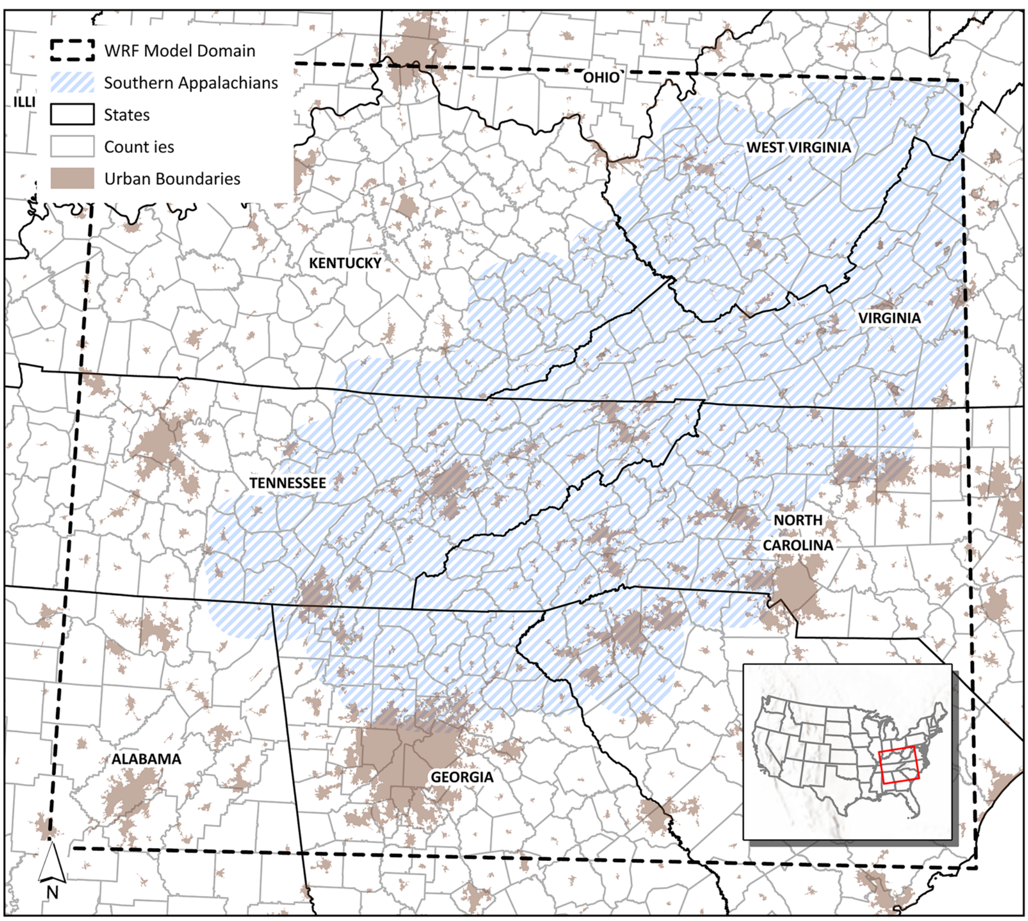

Fig. 6 | Southern Appalachian region in eastern North America, including the Weather Research and Forecasting (WRF–ARW) 500-m horizontal spatial resolution model domain, the evaluated region as defined by the 30-km buffer around the 700-m surface contour, and urban areas.

programming language, and ArcGIS Pro statistical mapping software was utilized in statistical and geospatial analyses of the selected events.

Data availability

The North American Model (NAM) forecast system reanalysis data used as forcing for WRF-AR can be found here https://www.ncei.noaa.gov/products/weather-climate-models/north-american-mesoscale. Version 4.3 of WRF-AR can be found here: https://github.com/wrf-model/WRF/releases. Model runs were conducted at Virginia Tech—https://www.docs.arc.vt.edu/resources/compute/00tinkercliffs.html.

Received: 6 March 2025; Accepted: 31 May 2025;
Published online: 26 June 2025

References

1. USGCRP. *Fifth National Climate Assessment*. (U.S. Global Change Research Program, Washington, DC, USA, 2023). https://doi.org/10.7930/NCA5.2023.
2. IPCC. 2023: Summary for Policymakers. In: (eds Core Writing Team, H. Lee, J. Romero) *Climate Change 2023: Synthesis Report.Contribution of Working Groups I, II and III to the Sixth Assessment Report of the Intergovernmental Panel on Climate Change*. (2023).
3. Eliassen, A. & Palm, E. On the transfer of energy in stationary mountain waves. *Geofys. Publ*. **22** (1960).
4. Durran, D. R. Downslope winds. Encyclopedia of atmospheric sciences. *Encycl. Atmos. Sci.* **2**, 69–74 (2015).
5. Smith, R. B. The influence of mountains on the atmosphere. *Adv. Geophys.* **21**, 87–230 (1979).
6. Durran, D. R. & Blumen, W. *Mountain Waves and Downslope Winds* https://doi.org/10.1007/978-1-935704-25-6_4 (1990).
7. Brinkmann, W. A. R. Strong downslope winds at Boulder, Colorado. *Mon. Weather Rev.* **102**, 592–602 (1974).
8. Lilly, D. K. A severe downslope windstorm and aircraft turbulence event induced by a mountain wave. *J. Atmos. Sci.* **35**, 1–23 (1978).
9. Gaffin, D. M. On high winds and foehn warming associated with mountain-wave events in the western foothills of the southern Appalachian Mountains. *Weather Forecast.* **24**, 53–75 (2009).
10. Cotton, W. R., Weaver, J. F. & Beitler, B. A. An unusual summertime downslope wind event in Fort Collins, Colorado, on 3 July 1993. *Weather Forecast.* **10**, 786–797 (1995).
11. Decker, S. G. & Robinson, D. A. Unexpected high winds in Northern New Jersey: a downslope windstorm in modest topography. *Weather Forecast.* **26**, 902–921 (2011).
12. Ashley, W. S. & Black, A. W. Fatalities associated with nonconvective high-wind events in the United States. *J. Appl. Meteorol. Climatol.* **47**, 717–725 (2008).
13. Knox, J. A., McCann, D. W. & Williams, P. D. Application of the Lighthill-Ford theory of spontaneous imbalance to clear-air turbulence forecasting. *J. Atmos. Sci* **90**, 3292–3304 (2008).
14. Doyle, J. D. & Durran, D. R. The dynamics of mountain-wave-induced rotors. *J. Atmos. Sci.* **59**, 186–201 (2002).
15. Klemp, J. B. & Lilly, D. K. The dynamics of wave-induced downslope winds. *J. Atmos. Sci.* **32**, 320–339 (1975).
16. Clark, T. L. & Peltier, W. R. Critical level reflection and the resonant growth of nonlinear mountain waves. *J. Atmos. Sci.* **41**, 3122–3134 (1984).
17. Clark, T. L. & Peltier, W. R. On the evolution and stability of finite-amplitude mountain waves. *J. Atmos. Sci.* **34**, 1715–1730 (1977).
18. Durran, D. R. Another look at downslope windstorms. part i: the development of analogs to supercritical flow in an infinitely deep, continuously stratified fluid. *J. Atmos. Sci.* **43**, 2527–2527 (1986).
19. Smith, R. B. & Sun, J. Generalized hydraulic solutions pertaining to severe downslope winds. *J. Atmos. Sci.* **44**, 29342939 (1987).
20. Vosper, S. B. Inversion effects on mountain waves. *Q. J. R. Meteorol. Soc.* **130**, 1723–1748 (2004).
21. Doyle, J. D. et al. An intercomparison of T-REX mountain-wave simulations and implications for mesoscale predictability. *Mon. Weather Rev.* **139**, 2811–2831 (2011).
22. Nation Weather Service (NWS) Morristown WFO. Mountain Wave High Winds. https://www.youtube.com/watch?v=NUjt5OfG6TA (2025).
23. Anderson, M. & Buckles, J. Classification of Mountain Wave Events across the southern Appalachians. In: *National Weather Association Conference* (Huntsville, AL, 2019).
24. Gaffin, D. M. An examination of the areal extent of high winds associated with mountain waves along the Western Foothills of the Southern Appalachian Mountains. *Natl. Weather Dig.* **35**, 48–55 (2011).
25. Gaffin, D. M. Foehn winds that produced large temperature differences near the southern Appalachian Mountains. *Weather Forecast.* **22**, 145–159 (2007).
26. Gaffin, D. M. *Unexpected Warming Induced by Foehn Winds in the Lee of the Smoky Mountains*. (2002).
27. Lindsay, C. V. Mountain waves in the Appalachians. *Mon. Weather Rev.* **90**, 271–276 (1962).
28. Kuligowski, E. D., Walpole, E. H., Lovreglio, R. & McCaffrey, S. Modelling evacuation decision-making in the 2016 Chimney Tops 2 fire in Gatlinburg, TN. *Int. J. Wildland Fire* **29**, 1120–1132 (2020).
29. Cook, K. & Rocky Mountain PBS. *Marshall Fire Ignited by Previously Buried Embers and Xcel Power Line, Investigators Conclude*. https://www.rmpbs.org/blogs/news/marshall-fire-cause-xcel-power-line-buried-embers (2023).
30. Powers, J. G. et al. The weather research and forecasting model: Overview, system efforts, and future directions. *Bull. Am. Meteorol. Soc.* **98**, 1717–1737 (2017).
31. Colle, B. A. & Mass, C. F. *High-Resolution Observations and Numerical Simulations of Easterly Gap Flow through the Strait of Juan de Fuca on 9-10 December 1995**.
32. Udina, M., Soler, M. R. & Sol, O. A modeling study of a trapped lee-wave event over the pyrénées. *Mon. Weather Rev.* **145**, 75–96 (2017).
33. Park, J. R. A numerical simulation of a strong windstorm event in the Taebaek Mountain Region in Korea during the ICE-POP. *Atmos. Res.* **272**, 1–19 (2018).
34. Oltmanns, M., Straneo, F., Seo, H. & Moore, G. W. K. The role of wave dynamics and small-scale topography for downslope wind events in southeast Greenland. *J. Atmos. Sci.* **72**, 2786–2805 (2015).
35. National Weather Service (NWS) Morristown WFO. *Watch, Warning & Advisory Criteria For NWS Morristown TN*. https://www.weather.gov/mrx/watchwarnadv (2025).
36. Chojnacki, A. L. Assessment of the risk of damage to 110 kv overhead lines due to wind. *Energies (Basel)* **14**, 1–14 (2021).
37. Bayani, R., Waseem, M., Manshadi, S. D. & Davani, H. Quantifying the risk of wildfire ignition by power lines under extreme weather conditions. *IEEE Syst. J.* **17**, 1024–1034 (2023).
38. Xue, H., Li, J., Qian, T. & Gu, H. A 100-m-scale modeling study of a gale event on the lee side of a long narrow mountain. *J. Appl. Meteorol. Climatol.* **59**, 23–45 (2020).

Acknowledgements

This research was supported with a subaward from the National Oceanic and Atmospheric Administration to the University Corporation for Atmospheric Research (NA16NWS4670042). UCAR Subaward No. SUBAWD002964 to Virginia Polytechnic Institute and State University.

Author contributions

All authors reviewed the paper. M.W. and B.J. wrote the main paper text. Z.C. provided Python code to parse through the WRF output. C.R. helped write the introduction and provided computing resources. D.H. and J.B. provided

the dates of the mountain wave wind events and helped provide literature of research on mountain waves in the Southern Appalachians.

Competing interests

No, I declare that the authors have no competing interests as defined by Nature Portfolio, or other interests that might be perceived to influence the results and/or discussion reported in this paper.

Additional information

Supplementary information The online version contains supplementary material available at https://doi.org/10.1038/s44304-025-00100-8.

Correspondence and requests for materials should be addressed to Marcus D. Williams.

Reprints and permissions information is available at http://www.nature.com/reprints

Publisher's note Springer Nature remains neutral with regard to jurisdictional claims in published maps and institutional affiliations.

Open Access This article is licensed under a Creative Commons Attribution 4.0 International License, which permits use, sharing, adaptation, distribution and reproduction in any medium or format, as long as you give appropriate credit to the original author(s) and the source, provide a link to the Creative Commons licence, and indicate if changes were made. The images or other third party material in this article are included in the article's Creative Commons licence, unless indicated otherwise in a credit line to the material. If material is not included in the article's Creative Commons licence and your intended use is not permitted by statutory regulation or exceeds the permitted use, you will need to obtain permission directly from the copyright holder. To view a copy of this licence, visit http://creativecommons.org/licenses/by/4.0/.

This is a U.S. Government work and not under copyright protection in the US; foreign copyright protection may apply 2025